A Self-Powered 2-Dimensional Motion Detection Chip

Zhijian Lu[1], Kwanlung Cheung[2], Tao Luo[3], Hongjiang Song[4] and Jennifer Blain Christen[5]

***Abstract*— We demonstrate a self-powered chip to detect motion which enables constant, non-invasive monitoring. The chip was implemented in a standard 0.18 μm CMOS process. A P-N junction photodiode array was fabricated in the chip to detect when light is blocked by the movement of a hand or finger. The interface circuit detects the change between the shadowing and the exposure to determine the specific movement. This entire chip operates without any off-chip power supply and provides digitized outputs including 1 bit direction output and an 8 bits output indicative of the velocity in two dimensions.**

I. INTRODUCTION

Motion detection plays an increasingly important role in many fields, especially mobile sensing. Since an external battery is not ideal energy source, researchers are driven to find innovative solutions. Energy harvest has become one popular solution to this problem. This technique involves absorbing energy from the surroundings to supply power to the system. Usually this is done by employing special processes, such as MEMS, or post-processing to add exotic materials [1]. We presents a technique for sensing movement which is driven by entirely by on-chip photodiodes fabricated in a standard CMOS process. The described chip facilitates both energy harvest and motion sensing. We are currently focusing upon hand gesture recognition applications. However, there are numerous applications that could benefit from a non-invasive, motion sensor power through energy harvesting including physical therapy and rehabilitation, kinesiology, body sensor networks, and fall detection [2]–[6]. Our work comprises a simple and reliable method to detect and record movement.

II. PHOTOSENSOR

A. Photodiode Cell

The photosensors used in this work consists of P-N junction photodiode cells; the photodiode configuration is shown in Figure 1. Each photodiode cell occupies a 100 μm $\times$ 100 μm area. These photodiodes are composed of the P+ layer and the N-well layer in a standard 0.18 μm CMOS process, and they absorb photons in the visible and near-infrared wavelength range. The current sources shown indicate the photocurrents generated by the corresponding photodiodes. The P+ layer is the current output node while N-well layer is shorted to P-substrate and grounded. As the simplest configuration of a photosensor, both the design and fabrication of the device are well-tested, and we are confident in the reliability of the devices.

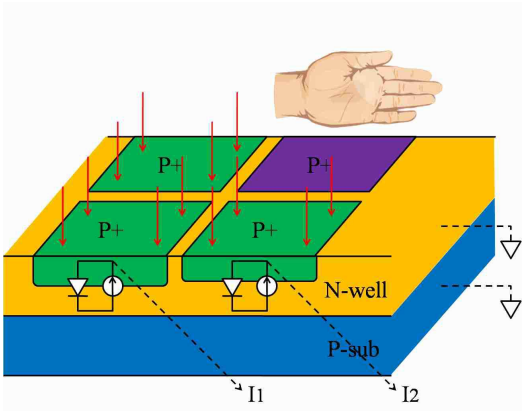

Fig. 1. An illustration of the on-chip photodetector used in this work.

B. TCAD Simulation

In order to properly design the devices to provide the necessary drive for the circuit, we performed a simulation of the device to determine the expected performance. These simulations informed the design of the chip. We used Silvaco Altas to simulate an on-chip photodiode cell at $T = 25°C$. The results allowed us to predict the behavior of the photosensors under both equilibrium and transient conditions. An I-V curve for a single photodetector is shown in Figure 2. Through these simulations we were able to determine numerous system properties such as a threshold voltage of 0.5 V and a slew rate of 10.6 $\mu A/V$.

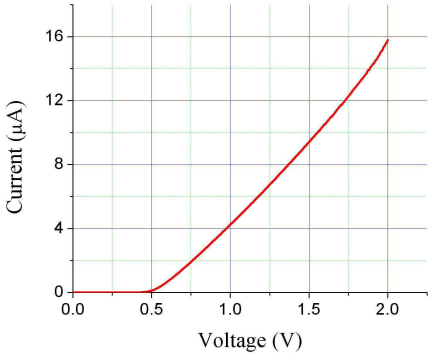

Fig. 2. Photodiode Cell I-V Curve from TCAD Simulations

*This work was supported by MOSIS

[1]Zhijian Lu, Tao Luo, Hongjiang Song, and Jennifer Blain Christen are with the School of Electrical, Computer and Energy Engineering, Arizona State University, Tempe, Arizona, 85287, USA Jennifer.Blainchristen at asu.edu

[2]Kwanlung Cheung is with Device Engineering Incorporated, Chandler, Arizona, USA

C. Photosensing Array

A photosensing array was created to detect motion in two dimensions as shown in figure 3. The on-chip array consists of 24 photodiode cells connected to facilitate motion sensing. Those cells are divided into two dimensions: Left / Right and Forward / Back. There are 4 types of cells in each dimension, e.g. L_1, R_1, L_2 and R_2 are in horizontal dimension Left / Right cells. In addition, the cells of each type are connected in parallel, e.g. all the L_1 cells are connected in parallel. The size of L_1 is twice as big as that of R_1, thus the photocurrent of I_{L_1} is double that of I_{R_1} when the chip is entirely exposed under known density light ranging from 45 mW/cm^2 to 95 mW/cm^2 simulating the scenario on the Arizona State University campus from 9 am to 5 pm in April.

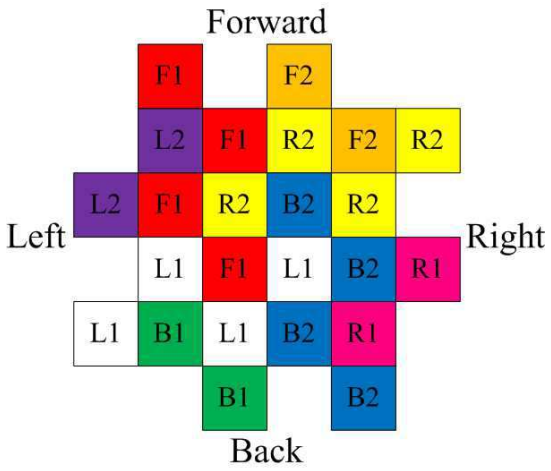

Fig. 3. Photodiode Sensor Array pattern is shown. The cell names indicate the sensing of the Left/Right (L_1, R_1, L_2 and R_2) and Forward/Back (F_1, B_1, F_2 and B_2) dimensions. Cells sharing a name are photodiodes connected in parallel.

D. Sensor Array Algorithm

We detect motion by sensing the movement above the chip. For instance, when a hand is moving above the chip it blocks the incident light. Thus, the photocurrent generated by each type of photodiodes changes because of the varying shadowing. It is apparent that the corresponding photocurrent is proportional to the exposed area of photosensor. We designed an interface circuit to compare the values of the photocurrents in 4 sets, $I_{L_1}\&I_{R_1}$, $I_{L_2}\&I_{R_2}$, $I_{F_1}\&I_{B_1}$ and $I_{F_2}\&I_{B_2}$.

For example, if a hand moves from left to right, at first, I_{L_1} is larger than I_{R_1} while I_{L_2} is smaller than I_{R_2}, due to the relative size. The shadowing increases from left to right until the hand covers the whole of L_2 and half of L_1. At that point, I_{L_1} is not larger than I_{R_1} while I_{L_2} is still smaller than I_{R_2}. The interface circuit generates a pulse depending on the comparison result between I_{L_1} and I_{R_1}. The shadowing continues increasing to cover the entire photosensor, but the comparison results remain the same even though there are tiny dark currents from the photosensor. After tens of milliseconds, the hand moves across the chip such that photodiodes are again exposed to light. Now, I_{L_1} is larger than I_{R_1} and I_{L_2} is larger than I_{R_2}. The exposure keeps increasing to expose the whole L_2 and half of L_1. Finally, I_{L_1} is still larger than I_{R_1}, but I_{L_2} is no longer larger than I_{R_2}. The interface circuit generates another pulse due to the comparison result between I_{L_2} and I_{R_2}. It is important to note that the pulse from $L_1\&R_1$ occurs prior to the pulse of $L_2\&R_2$. Figure 4 presents the sensor array outputs for the movement from left to right in horizontal dimension discussed above.

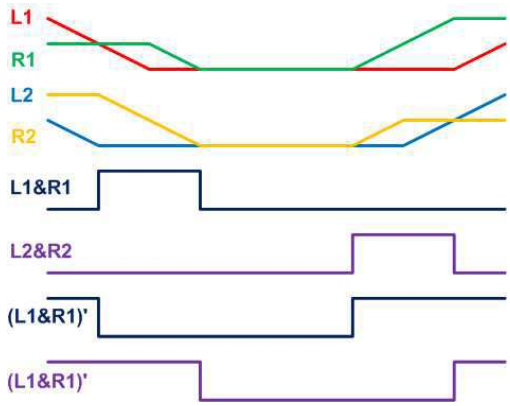

Fig. 4. The sensor array outputs demonstrating the algorithm for the movement from left to right in horizontal direction.

If a hand moves from right to left, it results in the reverse algorithm with the pulse of $L_1\&R_1$ following the pulse of $L_2\&R_2$ because of reflection symmetry in sensor array. Similarly, the algorithm in vertical direction can be achieved for rotational symmetry in sensor array shown in TABLE I.

TABLE I
SENSOR ARRAY ALGORITHM

Motion Types	Comparison Results
Left to Right	Pulse of $L_1\&R_1$ prior to Pulse of $L_2\&R_2$
Right to Left	Pulse of $L_1\&R_1$ after Pulse of $L_2\&R_2$
Forward to Back	Pulse of $F_1\&B_1$ prior to Pulse of $F_2\&B_2$
Back to Forward	Pulse of $F_1\&B_1$ after Pulse of $F_2\&B_2$

III. INTERFACE CIRCUIT IMPLEMENTATION

A. Architecture

Figure 5 shows the architecture of the interface circuit consisting of the on-chip power supply, photosensor array, current mirrors, comparator, clock generator and digital block. The signal flow is as follows: a hand moves above the chip causing shadowing over some parts of the sensing array. The photodiodes generate current to both drive the total power supply and indicate motion. An RC ring oscillator provides a 1 kHz clock frequency. Current mirrors convert currents from the photosensor array into voltages, which are measured by clocked comparators. Based on comparison results, there are two outputs generated in the digital block

after signal processing. The first output is a one bit indicator of the direction of the movement, and the second is the velocity of that motion represented with 8 bits.

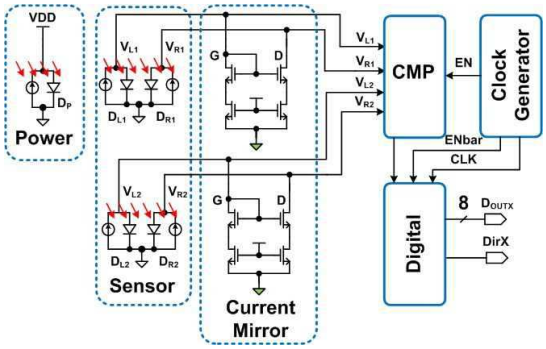

Fig. 5. Block diagram of the interface circuit

B. Clocked Comparator

A clocked comparator is used to compare the outputs from the photosensor array to implement the algorithm as described in TABLE I. Both the value and time interval for the results are used to generate the direction bit and the velocity data, respectively. The clocked comparator is seen in Figure 6. The circuit has an enable input (EN), and when EN is low, both OutP and OutN reset to high. When EN is high, the two inputs are compared, causing one of the outputs to be high while the other is low. The input voltages for this comparator must be over the threshold voltage of the NMOS devices for proper operation. Therefore, it works well when the sensor array is exposed to bright light or sunshine, which offers higher voltages. The comparator does not operate, conserving energy, when the sensor array is covered entirely by a hand, which offers only tiny voltages due to dark currents. In this situation, both outputs of the comparator remain unchanged and stay high.

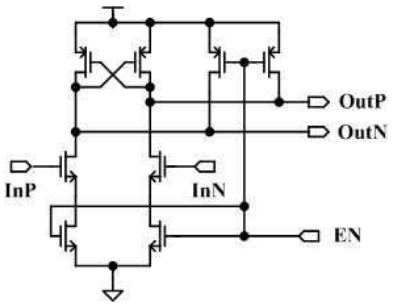

Fig. 6. Clocked comparator circuit

C. Digital Block

The key part of the interface circuit is the digital block. The digital block is responsible for creating the output from the comparator values. For each dimension, both the direction and the velocity are measured as digitized outputs

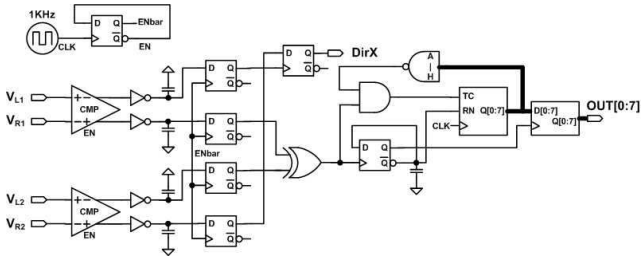

Fig. 7. Digital Block Schematic

D_{irX} and $Out[0:7]$ respectively. A schematic of the digital block is given in Figure 7.

For direction measurement, two pulses come from the photosensor array shown in Figure 3. We utilize a D flip-flop with rising edge trigger to compare the difference between two pulses. For instance $(L_1 \& R_1)'$ are connected to the D flip-flop's clock while $(L_2 \& R_2)'$ are connected to D flip-flop's data. If the movement comes from left to right, the output D_{irX} switches from 1 to 0. If the movement comes from right to left, the sequence between these two pulses is reverse because of reflection symmetry, hence the output D_{irX} switches from 1 to 0.

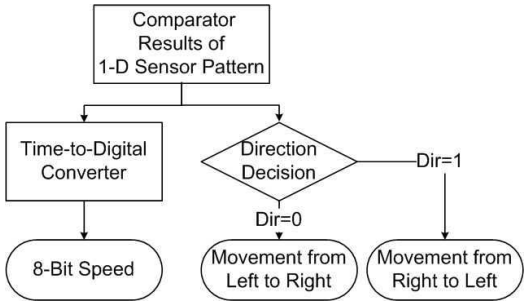

Fig. 8. Flow Chart for the Digital Block

To measure the velocity of the motion, a time to digital converter is used with operation shown in Figure 8. The circuit is used to measure the pulse width of the latter in the sequence, e.g. $L_2 \& R_2$ pulse width is converted to 8 bits digitized output. Overflow prevention is also considered in digital block, which indicates that the maximum output '1111 1111' can not be added to, since this would result in a '0000 0000' output. In addition, the relationship between the digitized output and the real speed is described as $v = \frac{d}{t} = \frac{400\mu m}{n \times 1ms} = \frac{0.4}{n} m/s$, where the distance is 4 photodiode cells' length i.e. 400 μm and the time is 1 kHz clock frequency multiplied by number of output bits, 8.

IV. LAYOUT, SIMULATION RESULTS AND SELF-POWER VERIFICATION

A. Layout

The complete chip layout is shown in Figure 9; it occupies 1.5 $mm \times 3$ mm for a total area of 4.5 mm^2 implemented in a standard 0.18 μm CMOS process. The majority of the chip area is dedicated to powering the chip, with significant

area also dedicated to the photosensing array. The digital circuits described section III are also visible in Figure 9.

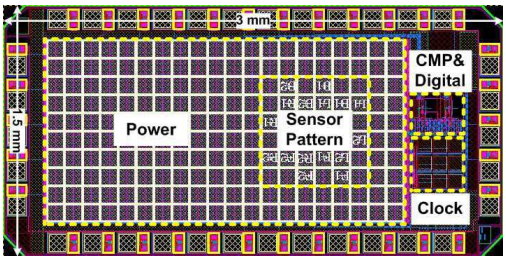

Fig. 9. Chip Layout

B. Simulation Results

The described system was simulated to determine the transient response to motion. We performed simulations of the chip in Cadence using current supplies to mimic the photocurrent in the system and power supplies set to estimated values derived from the photosensor TCAD simulations. One of the transient simulations with a power supply of Vdd = 0.4 V is shown in Figure 10 that demonstrates how the system would respond to motion in the horizontal direction. During the period from 0 ms to 60 ms, the movement comes from left to right. During the period from 60 ms to 120 ms, the movement comes from right to left. We can see that the plots for L_1/R_1 and L_2/R_2 give the response as would be expected for the horizontal motion as fully detailed in section II-D. In the four following waveforms, the digitized outputs generated by L_1, L_2, R_1, and R_2 are shown. The comparator outputs and inputs to the digital block are shown. Finally the clock signal followed by both the direction and velocity waveforms are shown. We can see a good match between the outputs and the expected results according to the algorithm in section II-D. From simulations, we have also determined the power consumption for the chip is 236 nW; this must be matched or exceeded by the power generated by the photosensor array.

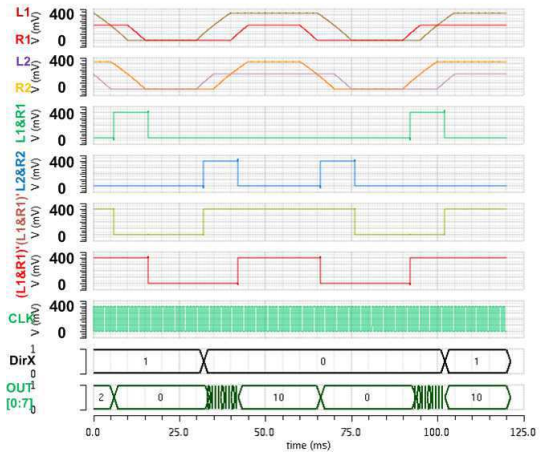

Fig. 10. Transient Simulation Waveform

C. Self-power Verification

The area of the chip dedicated to supplying power to the circuits is shown in Figure 9; it contains 176 photodiode cells occupying a total area of 1.76 mm^2. It is capable of generating a supply voltage from 400 mV to 489 mV under empirically determined optical power ranging from 45 mW/cm^2 to 95 mW/cm^2. These values were measured on the Arizona State University campus from 9 AM to 5 PM in April. If we assume that solar cell efficiency is 0.1, the minimum expected power provided by the photosensors is much larger than the power consumption of interface circuit calculated as $P_{min} = 45mW/cm^2 \times 0.1 \times 1.76mm^2 = 79.2\mu W$. In addition, our group has demonstrated self-powered optical sensing for solar tracking applications [7], [8], so we know the estimates are reasonable.

V. CONCLUSIONS

We have demonstrated a chip that is capable of sensing both the direction and velocity of motion near the chip. The chip uses a photosensor array to power the interface circuits that determine these values. While self-powered circuits using photosensors have been demonstrated previously [8], [9], the addition of motion sensing makes this chip particularly well-suited for gesture recognition. An array of these chips embedded in a desktop would allow for complex three dimensional gesture recognition. In the future we aim to target other applications in health care and wearable sensing such as study gait or to prevent falls, body sensor networks, and control of assistive technologies. Our goal was to create a motion sensing chip that was so small and light weight that it would not be noticed by the user.

REFERENCES

[1] Z. G. Wan, Y. Tan, and C. Yuen, "Review on energy harvesting and energy management for sustainable wireless sensor networks," in *Communication Technology (ICCT), 2011 IEEE 13th International Conference on*, Sept 2011, pp. 362–367.

[2] J. Meyer, P. Lukowicz, and G. Troster, "Textile pressure sensor for muscle activity and motion detection," in *Wearable Computers, 2006 10th IEEE International Symposium on*, Oct 2006, pp. 69–72.

[3] I. Pappas, T. Keller, S. Mangold, M. Popovic, V. Dietz, and M. Morari, "A reliable gyroscope-based gait-phase detection sensor embedded in a shoe insole," *Sensors Journal, IEEE*, vol. 4, no. 2, pp. 268–274, April 2004.

[4] S. Luo and Q. Hu, "A dynamic motion pattern analysis approach to fall detection," in *Biomedical Circuits and Systems, 2004 IEEE International Workshop on*, Dec 2004, pp. 1–5–8a.

[5] Z. Ding, I. Chen, S. Yeo, K. V. Ling, W. T. Wang, Z. Luo, and C. Lim, "Integration of sensing and feedback components for human motion replication," in *Body Sensor Networks (BSN), 2010 International Conference on*, June 2010, pp. 90–95.

[6] A. Chaudhary, J. L. Raheja, K. Das, and S. Raheja, "Intelligent approaches to interact with machines using hand gesture recognition in natural way: A survey," *CoRR*, vol. abs/1303.2292, 2013.

[7] H. Wang, T. Luo, H. Song, and J. Christen, "Cmos sensor for sun tracking," in *Sensors, 2013 IEEE*, Nov 2013, pp. 1–4.

[8] H. Wang, T. Luo, H. Song, and J. B. Christen, "On-chip sensor for light direction detection," *Optics letters*, vol. 38, no. 22, pp. 4554–4557, 2013.

[9] A. Fish, S. Hamami, and O. Yadid-Pecht, "Cmos image sensors with self-powered generation capability," *Circuits and Systems II: Express Briefs, IEEE Transactions on*, vol. 53, no. 11, pp. 1210–1214, Nov 2006.